RESEARCH ARTICLE | OCTOBER 15 2010

Epoxy-based nanocomposites for electrical energy storage. I: Effects of montmorillonite and barium titanate nanofillers

V. Tomer; G. Polizos; E. Manias; C. A. Randall

J. Appl. Phys. 108, 074116 (2010)
https://doi.org/10.1063/1.3487275

Epoxy-based nanocomposites for electrical energy storage. I: Effects of montmorillonite and barium titanate nanofillers

V. Tomer,[1,3] G. Polizos,[1,2] E. Manias,[2,a)] and C. A. Randall[1,b)]
[1]*Department of Materials Science and Engineering, Materials Research Laboratory, Center of Dielectric Studies (CDS), The Pennsylvania State University, University Park, Pennsylvania 16802, USA*
[2]*Department of Materials Science and Engineering, Polymer Nanostructures Laboratory, Center for the Study of Polymeric Systems (CSPS), The Pennsylvania State University, University Park, Pennsylvania 16802, USA*
[3]*The Dow Chemical Co., Corporate R&D, Midland, Michigan 48674, USA*

(Received 16 February 2010; accepted 7 August 2010; published online 15 October 2010)

Polymer nanocomposites prepared by epoxy reinforced with high permittivity barium titanate (BT) fillers or high aspect ratio montmorillonite (MMT) fillers exhibited marked changes in their high electric field properties and their relaxation dynamics, depending on the nanoparticle type and concentration, the nanoparticle size, and the epoxy matrix conversion. We investigated epoxy resin composites based on organically modified montmorillonite (oMMT) or BT ($BaTiO_3$) nanoparticles in order to delineate the effects of the high aspect ratio of the MMT and the high permittivity of the BT particles. We also explored the potential benefits of the synergy between the two fillers in systems consisting of epoxy and both oMMT and BT particles. It was observed that the nature of the organic–inorganic interfaces dominate the glass transition temperature and the dielectric properties of these composites. Specifically, using dielectric relaxation spectroscopy, we probed the local dynamics of the polymer at the interfaces. The MMT systems had approximately three orders of magnitude slower interfacial dynamics than those at the BT interfaces, indicating more robust interfaces in the MMT composites than in the BT-based composites; the corresponding energy barriers (activation energies) associated with these motions were also doubled for the MMT systems. Furthermore, we investigated the effect of the decreased glass transition, interfacial area, polymer-phase at the organic–inorganic interface, and of the dielectric breakdown on the electrical energy storage capabilities of these composites. © *2010 American Institute of Physics*.
[doi:10.1063/1.3487275]

I. INTRODUCTION

Advances in mobile electronic devices, stationary power systems, and hybrid electric vehicles demand compact and robust electrical energy storage solutions.[1–4] The introduction of inorganic nanoparticles into polymer matrices to form dielectric polymer nanocomposites represents one of the most promising and exciting avenues for compact and robust electrical energy storage solutions.[3–12] Such approaches capitalize on the idea that the amalgamation of inorganic materials of large permittivity with polymers of high breakdown strength may benefit the energy storage capacity, as energy density is directly proportional to permittivity and the square of the applied electric field.

Epoxy based nanocomposites have become the preferred choice of insulating materials for several electrical applications, including printed circuit boards, generator groundwall insulation system, and cast resin transformers. More recently these nanodielectric systems have become a strenuous topic of research for their energy storage capabilities, especially after the realized advantages of nanofillers resulting in improved properties, compared to the respective composites with micron-sized fillers.[7,13–26] Earlier studies have investigated various dielectric properties of epoxy nanocomposites including permittivity, tan delta values, ac voltage endurance, as well as short-term dc and ac dielectric strengths. At low field, the permittivities are observed to either increase or decrease as compared to that of neat epoxy.[23,27,28] An increase in permittivity is usually expected with high permittivity micro/nanofillers. However, examples in literature also demonstrated that a lowering of permittivity and of tan delta values is feasible, with nano-oxide fillers or layered nanosilicates, and was ascribed to the reduction in polar polymer chain mobilities.[20,29–31] High field results indicate impulse breakdown strengths to be higher with nanosized fillers when compared to micron-sized fillers.[27,32–34] In another work, improvements in time to breakdown are recorded in epoxy composites with Al_2O_3 nanofillers, which were also associated with interfacial responses.[35] Furthermore, it is reported that the insulation breakdown strengths in nanocomposites are less than that of the base epoxy, but they can be improved if silane coated nanofillers are utilized.[36] These observations in the electrical properties of epoxy nanocomposites are highly encouraging and they are mainly attributed to the unique properties of nanoparticles and the dynamics at the interfacial region.[8,9,20,29,31,37–40] Thus, dielectric performance can be tailored through proper filler and interface design and, thus, enable the utilization of epoxy nanocomposites for electrical energy storage. In this sequence of two papers, we

a)Electronic mail: manias@psu.edu.
b)Electronic mail: car4@psu.edu.

demonstrate that nanocomposite materials can exhibit improved energy storage. However, the dielectric properties of the matrix-filler interfaces were found to be the limiting factor for achieving large energy storage, primarily due to the effects of molecular motions changing dramatically within a relatively short range (i.e., promoting an electric breakdown dominated by electronic breakdown in the regions where molecular motions are hindered, cf. at the interfaces, whereas further away from the fillers electromechanical or thermal breakdown is more probable, similarly to unfilled polymers). So, it becomes critical to appropriately design the polymer-filler interfaces to achieve high dielectric performance nanocomposites.

From a more fundamental perspective, experimental and simulation results indicate that the lowering of the glass transition temperature (T_g) in epoxy nanocomposites can be ascribed to the presence of a dual nanolayer polymer-filler interface:[23,29,31,39] In the simplest approach, the first layer can be envisioned as the highly-immobile organic fraction (assumed to be tightly bound and exist closest to the nanoparticle surface), whereas the second interfacial layer, containing the faster relaxing species (loosely bound polymer chains), is envisioned to reside just beyond the first layer. Although experiments[13,41] and simulations[13,42–45] have demonstrated that this may be an over-simplified picture, it is commonly used as a qualitative description for the filler-induced changes in dynamics and T_g. In any case, it remains quite clear that the dielectric properties of the nanocomposite shall be largely dictated by this dual-dynamics interfacial region around each nanoparticle and, hence, the filler character and loading should play a significant role on the final performance of the composite. However, most of the existing literature explores the various parameters—including filler effects, glass transition temperature (T_g), permittivity, and low and high-field behavior—separately, with no established understanding of the interrelations between these parameters; for example, how would the confinement-altered polymer dynamics and T_g—or even the presence of extensive polymer-filler interfaces—affect the space charge development and further determine the dielectric breakdown strength.

This work focuses on establishing such correlations based on experimental data, so as to ultimately lead to the design/development of high performance polymer nanocomposites for electrical energy storage applications. The filler loading and geometry, as well as the processing conditions, are expected to influence the macroscopic properties of the composites; thus, it is important to investigate the benefits, if any, for epoxy nanocomposites with nanofillers differing in permittivity and in aspect ratio. Specifically, we focus on nanocomposites of epoxy matrix with two selected nanofillers: $BaTiO_3$ (BT) and organically modified montmorillonite (oMMT). Structure-property relationships between the morphology of the composites, crosslinking density, and filler surface modification are established for the low and high field properties, such as conductivity, dielectric breakdown strength, and recoverable energy density; particular emphasis is given on the effects of the polymer-filler interfacial properties.

II. EXPERIMENTAL

A. Materials

Hybrid organic/inorganic (nano)composites were prepared by dispersing barium titanate (BT) and/or oMMT clay particles in epoxy resin. Typical (single-filler) nanocomposites were obtained when a single inorganic constituent—either BT or oMMT—was dispersed in the epoxy matrix, whereas dual-filler composites were obtained by a simultaneous dispersion of both inorganic components in the organic matrix.

For the inorganic oMMT and BT phases, commercial available materials were used: Nanomer I30E MMT (Nanocor, IL) with cation exchange capacity of about 1.4 meq/g and an organic loading of octadecyl-ammonium surfactant of about 30 wt %; $BaTiO_3$ powder (hydrothermal BT-8, Cabot Performance Materials, Boyertown, PA) having a Ba/Ti ratio of 0.998 and a median particle size of 0.15 μm. Surface treatment of the $BaTiO_3$ particles with (3-glycidoxypropyl)trimethoxysilane (Gelest) was carried out as follows: 12 g of purified (leached) BT powder were suspended in a solution of 90 ml ethanol, 10 ml distilled water, and 0.6 g of (3-glycidoxypropyl)trimethoxysilane; the mixture was stirred for 24 h, subsequently centrifuged for 10 min and finally the precipitated modified powder was dried at 120 °C for 6 h.[46,47]

The composites were prepared by adding the fillers into an epoxy resin (diglycidyl ether of bisphenol-F, Epon 862, Hexion Specialty Chemicals). The dispersion of the particles was aided by high shear mixing and sonication of the suspension. The suspensions were charged with appropriate amounts of crosslinker, 2-ethyl-4-methylimidazole (Curing Agent Imicure™ EMI-24), and were degassed under vacuum to remove any trapped air. Films 100 μm thick were obtained by casting the solutions between teflon plates and placing them on a hot plate to accelerate the curing process (the samples were cured at 60 °C for 3 h, and postcured at 180 °C).

B. Instrumentation

1. Transmission electron microscopy

A Leica Ultracut UCT Microtome with cryoattachment was used for sectioning the specimens. The microtomed samples were tested under a transmission electron microscope (TEM, Jeol JEM-2010 with LaB_6 emitter) operated at an accelerating voltage of 200 kV.

2. Thermogravimetric analysis (TGA)

TGA measurements were performed on a Thermal Analysis (TA) Instruments SDT Q600 analyzer under nitrogen environment. The temperature ramps were from 20 to 1000 °C at a heating rate of 10 °C/min.

3. Differential scanning calorimetry (DSC)

DSC data were collected on a TA Q200 calorimeter in a gas mixture of nitrogen and helium. The measured heat flow was obtained at a cooling temperature ramp of 5 °C/min. The temperature accuracy was 0.1 °C. For monitoring the

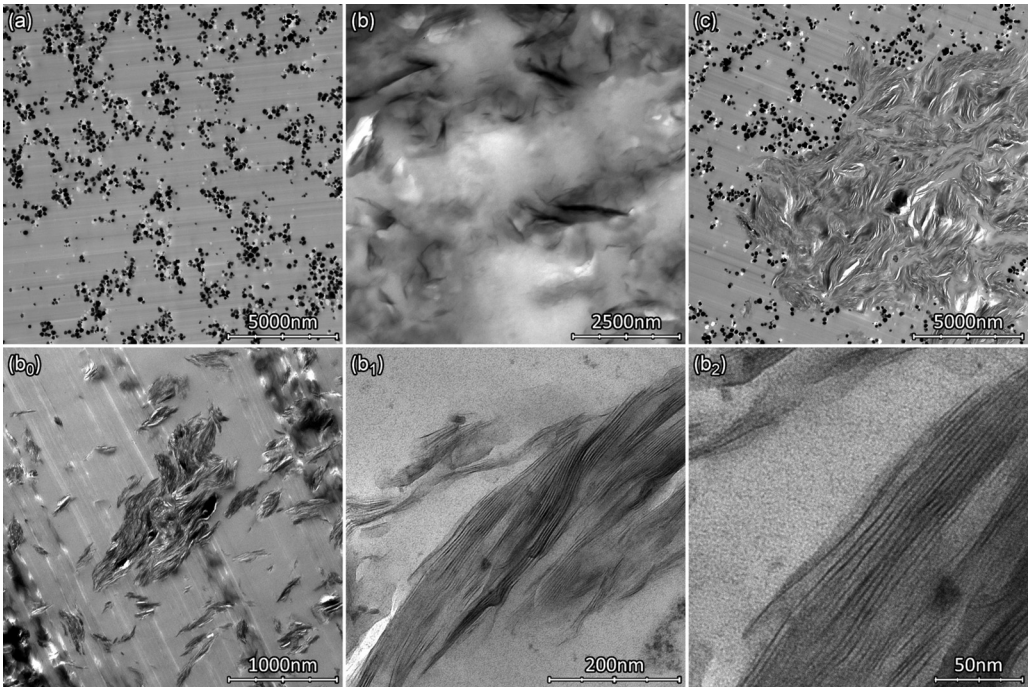

FIG. 1. First row: representative TEM images of the investigated epoxy-based composites with (a) 10 vol % $BaTiO_3$; (b) 6 wt % oMMT; (c) 10 vol % $BaTiO_3$ and 3 wt % oMMT. Second row: TEM images of selected structures within the epoxy/6 wt % oMMT composite: (b_0) one of the largest MMT nanoplatelet agglomerations in the epoxy/oMMT system, exemplifying that the largest filler assemblies in this system are five to ten times smaller compared with the morphologies of the dual-filler (10 vol % $BaTiO_3$ and 3 wt % oMMT) composites shown in (c); (b_1) and (b_2) higher magnification images from oMMT assemblies, showing that the nonexfoliated oMMT platelets are well-intercalated by polymer.

glass transition, high to low temperature ramps, with or without temperature modulation, were performed in order to follow the same thermal sequence as in the dielectric spectroscopy experiments. The postcuring temperature of the specimens was defined by the completion temperature of the epoxy matrix curing reaction. For the data analysis, the TA universal analysis software was used.

4. Dynamic mechanical analysis (DMA)

DMA measurements were carried out on a TA Q800 instrument. Sample stripes (15 mm in length, 6 mm in width, and 200 μm thick) were measured in the tensile mode at a frequency of 1 Hz. The temperature ramps were performed under 1 MPa stress (well within the linear region in the stress-strain curves) and at a 4 °C/min heating rate.

5. Dielectric relaxation spectroscopy (DRS)

DRS experiments were performed over broad frequency (10^{-2} to 10^6 Hz) and temperature (180 to 100 °C) ranges. Disklike specimens, about 100 μm thick and 20 mm in diameter, were sandwiched between gold-sputtered brass electrodes and mounted on a Novocontrol ZGS Alpha active sample cell, which was connected to a Novocontrol Quatro Cryosystem for temperature stabilization (±0.1 °C). Prior to the DRS measurements, the samples were equilibrated in the cell at 100 °C for 30 min to eliminate bulk water contributions to the spectra and to facilitate similar conditions in all the systems measured. The real and imaginary parts of permittivity [$\varepsilon^*(\omega)=\varepsilon'(\omega)-i\varepsilon''(\omega)$, where ω is the angular frequency, $\omega=2\pi f$] were collected isothermally in the order of decreasing temperature. A more detailed description of the data analysis has been presented elsewhere.[11,12,48]

6. Displacement-electric field loops

High-field polarization-electric field loops were recorded with a modified Sawyer–Tower circuit. The samples were subjected to two successive sine waves, with frequency of 1 Hz. The polarization-electric field loops are presented according to the data from the second cycle.

7. Dielectric breakdown strength

Dielectric breakdown measurements were performed on a TREK P0621P instrument. The samples were sandwiched between a one-side conducting polypropylene tape (top electrode) and a copper plate (bottom electrode). All the specimens were tested at room temperature under a dc voltage ramp of 500 V/s (more details can be found elsewhere[11,12]).

III. RESULTS AND DISCUSSION

A. Structural analysis

TGA, TEM, DSC, and infrared (IR) techniques were employed in order to assess the organic loading of the fillers, their dispersion, and the effect of the inorganic phase on the glass transition temperature and the crosslinking density of the polymeric network. TGA analysis depicted the organic loading to be approximately 30 wt % and 2.7 wt % for the oMMT and silanated-$BaTiO_3$ particles, respectively, according to the plateau values at temperatures higher than 800 °C.[53] For the oMMT, an abrupt weight loss at temperatures higher than 250 °C was attributed to the decomposition

of the alkyl-ammonium surfactants, a process which occurs concurrently with the dehydration of the silicate plates.[49] The purified (as received) BT particles have significantly lower organic content, which was estimated by comparing the residual values before and after BT silanization, and was found to be around 1.5%.

The nanostructures obtained for the three composites are presented in Fig. 1. Both single-filler composites demonstrate good dispersions, in concert with the thermodynamically favorable polymer-filler interactions between the polar polymeric matrix and the inorganic filler surface (e.g., Lewis acid/Lewis base interactions[49–51]) and the processing approach. Specifically, dispersed $BaTiO_3$ spherical particles (0–3 composites[11,52]) are observed in Fig. 1(a), with a mostly random dispersion of fillers; at the nanometer scale there seems to exist some local clustering of BT particles but almost all BT particles are separated by epoxy matrix (i.e., there is no considerable BT agglomeration). For the epoxy/oMMT composites the typical intercalated/exfoliated mixed morphology is obtained, with the smaller platelets being well-dispersed (exfoliated) in the organic matrix, while the larger platelets are in intercalated structures mostly consisting of five to ten individual MMT layers [Fig. 1(b)]. Given the chemical inhomogeneities of the naturally-occurring MMT and the processing approach used (mechanical mixing followed by sonication) there still exist few micron-sized intercalated oMMT agglomerates (one of the largest ones found in the TEM study is shown in Fig. 1(b_0), containing a few hundreds of MMT layers) however even the largest of these filler structures are about ten times smaller than those obtained for the dual-filler (BT and oMMT) composites [cf. Fig. 1(c), *vide infra*]. The larger filler structures that exist in significant numbers in the epoxy/oMMT composites are those of the intercalated larger-size MMT layers mostly consisting of tens of individual MMT layers [Fig. 1(b)], and where the individual MMT platelets are separated by approximately 2 nm of polymer inserted within the oMMT inter-gallery spacings [Fig. 1(b_1) and 1(b_2)]. In contrast, the dual-filler BT and oMMT composites exhibit a strongly phase separated structure [Fig. 1(c)], where evidently the presence of BT in the epoxy matrix leads to a high agglomeration of the oMMT layers in extended multimicrometer sized domains containing thousands of MMT layers. The origins of this phase separated morphology were traced to the difference in interactions between the epoxy and the two fillers,[53] which can be overcome by reacting the two fillers prior to introducing them to the epoxy (this is the focus of the second paper of this series, for more details see[53]).

Figure 2 shows the DSC curves for the various composites, and the summarized values are presented in Table I. An implicit correlation between the filler loading and the glass transition temperature, T_g, of the polymer matrix is observed, with a systematic decrease in T_g values with increasing inorganic content of both BT and oMMT. Such a T_g lowering can be caused by the disruption of the epoxy crosslinking due to the fillers. For example, epoxy/oMMT composites exhibited a more pronounced T_g decrease, as expected from the higher surface area of the MMT fillers. The maximum T_g decrease was found to be approximately 9% (for the 6 wt % oMMT and for the 30 vol % BT composites). In the dual-filler system (10 vol % BT and 3 wt % oMMT) despite the phase separated morphology, shown in Fig. 1(c), only one glass transition temperature was observed; this T_g coincides with the T_g of the 3 wt % oMMT composite but maybe due to the superposition the two similar T_g values from the two phases. Interestingly, the T_g values for the 10 vol % silane treated BT composite were comparable to the matrix. This result indicates an improvement in the interfacial characteristics, especially better crosslinking density, for the BT composites.

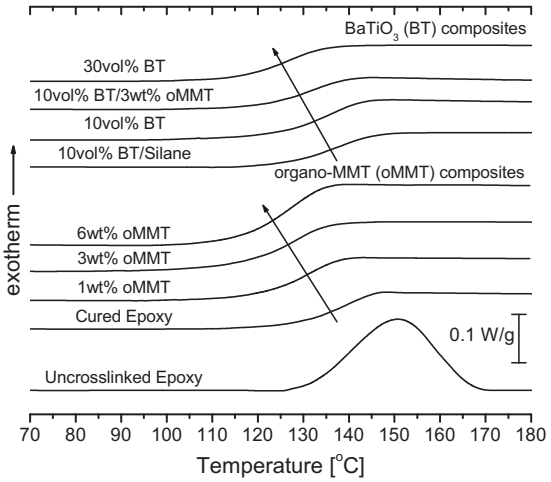

FIG. 2. Summarized DSC curves of the cured epoxy matrix and of the composites at several filler loadings. The curves (cooling rate 5 °C/min) are baseline corrected and heat flow is normalized by the epoxy weight, rather than by the specimen weight. The arrows indicate the direction of glass transition temperature decreasing, and the curves are shifted vertically for presentation clarity.

Infrared spectroscopy was employed to further investigate the crosslinking density of the polymer matrix. The relevant bands of the spectra corresponding to the oMMT composites, along with those of the uncrosslinked and crosslinked epoxy matrices, are shown in Fig. 3. The existence of uncrosslinked epoxide groups is manifested by the absorbance peak at 910 cm^{-1}, corresponding to the antisymmetric deformation of unreacted epoxide rings. After correcting the baseline and normalizing the intensity (the peak intensity of the aromatic ether alkyl C–O band at 1034 cm^{-1}

TABLE I. Summarized calorimetric glass transition temperatures derived from the corresponding DSC curves in Fig. 2. The reported T_g values were obtained from cooling (high to low temperature) ramps, and the associated errors are smaller than 0.3 °C (depending on baseline configuration).

Sample	T_g (°C)
Epoxy matrix	139.4
1 wt % oMMT	131.3
3 wt % oMMT	128.9
6 wt % oMMT	127.1
10 vol % $BaTiO_3$	137.6
10 vol % $BaTiO_3$/silane	139.3
10 vol % $BaTiO_3$/3 wt % oMMT	129.8
30 vol % $BaTiO_3$	126.7

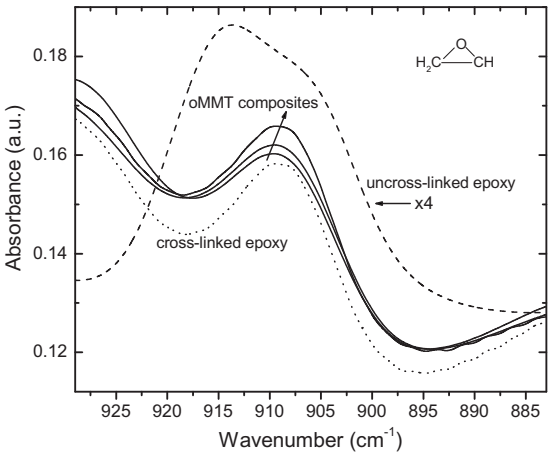

FIG. 3. Attenuated total reflectance IR spectra of the oMMT composites (solid lines) along with the uncrosslinked (dashed line) and the crosslinked (dotted line) epoxy. The peak intensities are background corrected and normalized, the arrow indicates the direction of increasing oMMT filler loading (1, 3, and 6 wt % oMMT) in the composites.

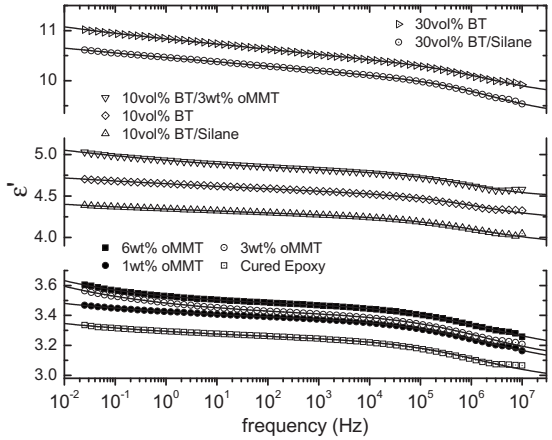

FIG. 4. The real part, ε', of permittivity over the measured frequency range for the $BaTiO_3$ and oMMT composites as indicated on the plot. The lines are the best fits to the experimental data. Measurements were performed at 20 °C, after postcuring the samples at 180 °C.

used as a reference) the area of the 910 cm^{-1} peak is shown to increase systematically with higher oMMT content. This behavior indicates an increasing deficiency of the organic phase to crosslink due to the presence of the inorganic oMMT phase, a behavior that becomes more pronounced at higher filler loadings (i.e., increasing systematically between composites with 1, 3, and 6 wt % in oMMT). This same trend is also reflected in the variation in the glass transition temperature of the polymer network (as shown in Fig. 2 and Table I), as expected: Since an increase in the uncured phase (regions of higher segmental mobility) would induce faster dynamics in the network ("plasticizing" effect) and consequently would lead to a decrease in the T_g. The crosslinking rate of the composites can also be estimated.[54] Namely, after normalizing the integrated 910 cm^{-1} absorbance band by the area of the 1034 cm^{-1} phenyl group band and accounting for the filler volume fraction, the crosslinking rate was calculated to vary from 89% to 94% for all systems studied. In the composites incorporating BT fillers, a similar systematic variation between the BT loadings and the IR peak areas could not be established experimentally, most probably due to the strong absorbance background of BT in the 1000 cm^{-1} region.[55,56]

B. Dielectric properties under low electric field

1. Permittivity characterization

The comparison plot of the real part of permittivity, $\varepsilon'(f)$, for all the samples at 20 °C (room temperature) is shown in Fig. 4. Fitting to the data was carried out simultaneously in both real and imaginary spectra of the complex permittivity function; in addition, to account for the low frequency polarization effects (linear divergence), a superposition of a power law contribution was also taken into account. The extracted static permittivity, ε_s, values were found to be in good agreement with the measured ε' values at 1 Hz, and the latter are summarized in Table II (ε'(1 Hz) data was preferred in order to eliminate fitting uncertainties arising from the dipolar relaxation in the high frequency region, a process which appears as a step in the $\varepsilon'(f)$ dispersion function at the same frequency regime for all the samples). In contrast to BT, the presence of oMMT fillers in the polymer matrix does not significantly increase the ε_s value of the composites, primarily due to the similar permittivity values of matrix and MMT filler. Interestingly, addition of surface-modified BT fillers results in a slight decrease in ε_s (in both 10 and 30 vol % composites) compared to the corresponding unmodified-BT systems. Given the high permittivity of the BT inorganic, this behavior can only be explained by assuming the formation of a lower permittivity polymer layer (shell), located between the filler surface and the crosslinked epoxy matrix (cf. core-shell model[57]). For BT fillers without surface modification, this shell will consist of unreacted and highly polarizable polymer chains with epoxide rings. The epoxy/modified-BT interface, with cyclic ether (epoxide) silane groups, should bear a resemblance to the crosslinked polymer phase and therefore the ε_s value of the shell decreases depending on the conversion rate (due to the small changes in the permittivity ~0.3–0.4 and due to uncertainties arising from the volume fraction and the density state of the polymer shell phase, a quantitatively analysis in terms of mixing rules was not attempted here). Based on this phase model, it is anticipated that differences in crosslinking and in polymer-filler interactions will give rise to polymer states with different dynamics.[44,45] In order to probe these dynamics directly, including their dependence on the filler type and

TABLE II. The real part of permittivity (ε') at 1 Hz for all systems.

Sample	ε' at 1 Hz
Epoxy matrix	3.3
1 wt % oMMT	3.4
3 wt % oMMT	3.5
6 wt % oMMT	3.5
10 vol % $BaTiO_3$	4.7
10 vol % $BaTiO_3$/silane	4.3
10 vol % $BaTiO_3$/3 wt % oMMT	4.9
30 vol % $BaTiO_3$	10.9
30 vol % $BaTiO_3$/silane	10.5

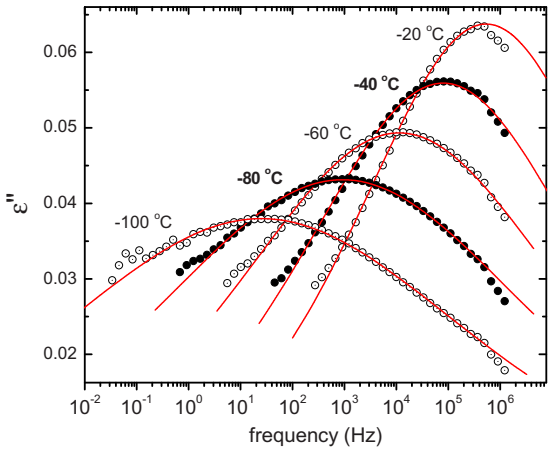

FIG. 5. (Color online) Dielectric loss data vs frequency for the 10 vol % $BaTiO_3$/3 wt % oMMT dual-filler composite, focusing on the relaxation peak for selected temperatures as indicated on the plot. The lines are the best fits to the data.

concentration, DRS measurements were performed at temperatures below and above the T_g, which would allow for identifying the correlations to the macroscopic conduction and to the space-charge processes, respectively.

2. DRS at temperatures below T_g

The low temperature relaxation process of the unfilled epoxy and a number of binary and ternary composites is shown in Fig. 4 through the $\varepsilon'(f)$ dispersion spectra, and examples of representative loss spectra as a function of temperature are given in Fig. 5, using the 10 vol % BT/3 wt % oMMT dual-filler composite as a representative system. The best fitting analysis was achieved by a Cole–Cole dielectric function:[58,59]

$$\varepsilon^*(\omega) = \varepsilon_\infty + \frac{\Delta\varepsilon}{1 + (i\omega\tau_{\max})^{1-\alpha}}, \quad 0 < (1-\alpha) \leq 1, \qquad (1)$$

where ω is the angular frequency; $\tau_{\max}$ is the characteristic time corresponding to the frequency of the loss peak maximum ($1/\tau_{\max} = 2\pi f_{\max}$); $\Delta\varepsilon$ is the dielectric relaxation strength [with ε_s and ε_∞ defined as the low and high frequency limits of the $\varepsilon'(\omega)$]. The shape parameter α is associated to the slopes of the $\varepsilon''(\omega)$ function at the low and high frequency limit with respect to the maximum frequency of the mode. For all measured temperatures, both the shape parameter α and the relaxation frequency $f_{\max}$ (i.e., the frequency corresponding to the midpoint of the permittivity ε' step and to the peak maximum of the loss ε'') were found to have identical values in all measured specimens; thus, the data from only one representative system are shown in Fig. 5. The origin of this mechanism is attributed to the local relaxations of the crosslinked phase, which is evidently characterized by the same local environment in all the samples, as will be discussed later.

In the temperature range between 40 °C and T_g, a new relaxation mode was identified in the composites containing sufficiently high polymer-filler interfacial areas [as shown in Fig. 6(b) at a representative temperature of 90 °C]. This new relaxation is evident for the composites with 3 and 6 wt %

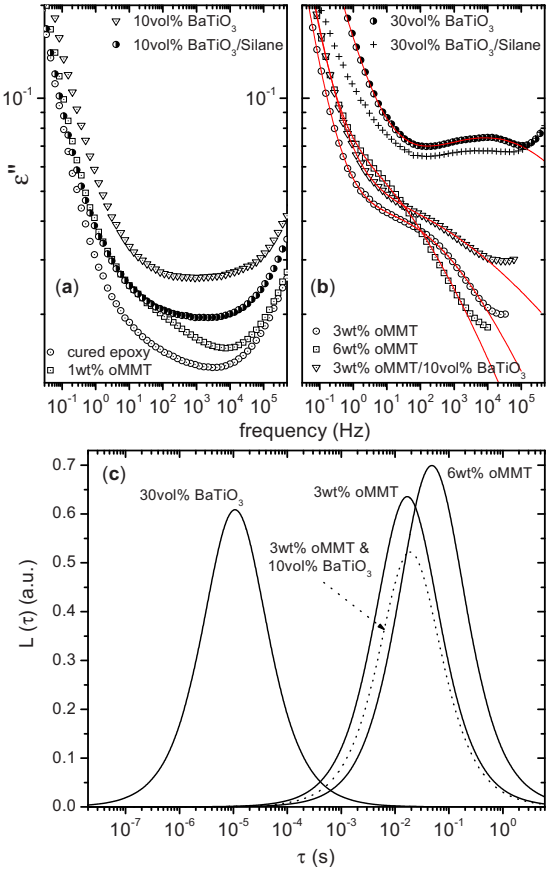

FIG. 6. (Color online) (a) Summary dielectric loss plots for the pure epoxy matrix, along with the composites with both filler types at low filler content. (b) By increasing the filler volume fraction a new relaxation process is revealed. Best fitting to the dipolar contribution was obtained by a Cole–Cole dielectric function [Eq. (1)], and (c) provides the corresponding distribution of relaxation times. All data sets were obtained at T=90 °C.

oMMT, 30 vol % BT, and the dual-filler phase-separated system with 10 vol % BT and 3 wt % oMMT, whereas it is absent in the unfilled crosslinked epoxy matrix as well as in the 1 wt % oMMT and 10 vol % BT composites [Fig. 6(a)] at the same temperature. Therefore, it is natural to ascribe this process to an interfacial mechanism, originating from the relaxation of polar groups at the polymer-filler interfaces. In view of the IR results that demonstrate the existence of uncrosslinked phase in the composites, it is very reasonable to attribute the state of those relaxors to unreacted (mobile) epoxy monomers, possibly located in the vicinity of the inorganic fillers. For the oMMT composites this process may be commensurate with the interfacial dynamics of the MMT-bound cationic surfactants. However, it should be noted that this new mode only manifests in the composites with high filler surface areas [as those in Fig. 6(b)], whereas it is absent in the DRS of the unfilled epoxy and the composites with lower interfacial area [Fig. 6(a)], despite the IR detection of uncrosslinked phases in these systems. This behavior most probably arises from a low population of relaxing groups in these later systems (that would result in a weak dielectric relaxation strength, $\Delta\varepsilon$), which, in turn, would result in this mode being masked by the conductivity contribution in the loss data. In other words, we believe that this mode is still present in the systems with lower interfacial area but it is too

weak to be detected by DRS. Finally, surface modification of the BT fillers was found to improve the interfacial properties; thus, even for the highest BT inorganic concentration studied (30 vol % BT composite), silane modification of the fillers apparently suppresses the dielectric relaxation strength of this interfacial process, which becomes negligible [Fig. 6(b)]. Thus, the surface functionalization appears to be promising for integrating multiphase composites and for preventing the formation of weak interfaces.

The composite with 30 vol % unmodified BT exhibits distinct dynamics compared to the oMMT composites, as shown in Fig. 6(b), with the dielectric mode of the oMMT composites occurring at lower frequencies (longer relaxation times). A better illustration of this same response is given in Fig. 6(c) by showing the corresponding distributions of relaxation times [$L(\tau)$ (Refs. 58 and 59)] comparing the composites with BT against those with oMMT fillers. Assuming that the broadening of the mode is due to the superposition of Debye processes, $L(\tau)$, the loss spectrum would be

$$\varepsilon''(\omega) = \int_{-\infty}^{\infty} \frac{\omega\tau L(\tau)}{1+(\omega\tau)^2} d\ln(\tau), \tag{2}$$

where $L(\tau)$ can be calculated from the fitting parameters of the imaginary part of permittivity and can be written analytically as:[58]

$$L(\tau) = \frac{1}{2\pi} \frac{\sin(\pi - \alpha\pi)}{\cosh(\ln\tau - \ln\tau_0) + \sin(\pi - \alpha\pi)}. \tag{3}$$

Noticeably, the dynamics of the oMMT composites are about three orders of magnitude slower than those of the BT composites, as manifested by the time distribution shift toward longer relaxation times. This dynamical behavior is a clear evidence of the difference in the dynamics of the physisorbed (restricted mobility) polymer on the MMT surface, indicating a more coherent and robust interface for the epoxy/oMMT than for the epoxy/BT. Similar to our previous studies,[11,12] the symmetric Cole–Cole distribution function is suggesting independent (isolated) relaxors that probably originate from good dispersion of the fillers. The composites with 3 wt % in oMMT demonstrate similar dynamics independent of the BT presence (i.e., the distribution of relaxation times is not affected by the presence of the 10 vol % BT filler), whereas increasing the oMMT filler loading results in longer relaxation times (i.e., the relaxation time distribution of the 6 wt % oMMT composite is shifted to longer relaxation times compared to the 3 wt % oMMT systems). The raw spectra clearly indicate that this new mode relates to interfacial species at the oMMT tactoids. Further, we can safely assume that the detected relaxation originates from the average dielectric response (non-Debye) of organic species at the oMMT interfaces (including hydroxyl groups, formed during the epoxide ring conversion, which can hydrogen bond to the MMT silicate surface), then the observed retardation in the dynamics of the 6 wt % oMMT reflect an increase in the population of the epoxy groups attached to the MMT, due to the increase in the cluster's surface area.

The processes of Fig. 6(b) were followed by DRS over a broad temperature range, and the corresponding relaxation

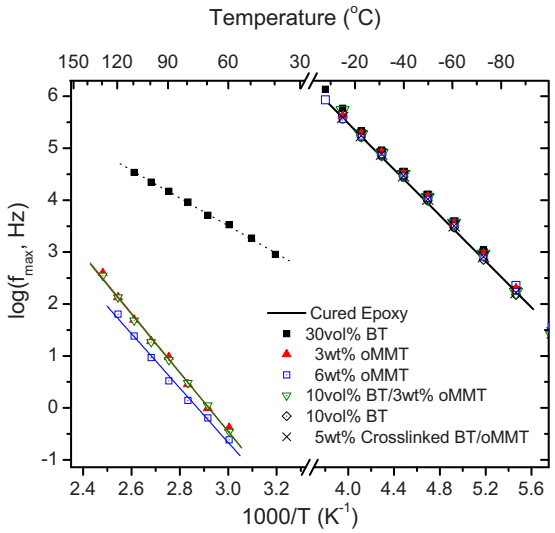

FIG. 7. (Color online) Arrhenius plot for all the relaxation processes obtained at temperatures below the glass transition temperature; composites exhibit two distinct modes, whereas the unfilled epoxy shows only one. The ultra-fast modes (in the subzero temperature range, assigned to the epoxy that is unaffected by the fillers) were found to overlap across all systems/compositions, including a composite with a 5 wt % reactive fillers [BT covalently-bonded (crosslinked) to oMMT (Ref. 53)]. The lines are best linear fits to the data.

frequencies, f_{max}, versus the reciprocal temperature are shown in Fig. 7. For comparison, we added in the same plot the local relaxations due to the crosslinked epoxy matrix, which were detected in the subzero temperature range (cf. Fig. 6). This latter mode, which is common for all systems, exhibits dynamics that are several orders of magnitude faster compared to the dynamics arising from the interfaces. These faster modes were found to be similar across all systems, and therefore independent of the filler phase (oMMT or BT) and of filler loading; this behavior further justifies our assignment of this mode to the crosslinked epoxy phase which remains unaffected (located far away) from any fillers.

The temperature dependence of f_{max} for all the relaxations in Fig. 7 is described well by the Arrhenius equation:[58,59]

$$f_{max}(T) = f_\infty \exp\left(-\frac{\Delta E_A}{k_B T}\right), \tag{4}$$

where ΔE_A is the corresponding activation energy; f_∞ is the relaxation rate in the high temperature limit; and k_B is the Boltzmann constant. Using Eq. (4), the calculated activation energy for the fastest mode was found to be 42 kJ/mol. This is in good agreement with previous studies reported in the literature, which ascribed it to local relaxations of hydroxyl groups in the crosslinked epoxy network.[60] For the composite systems of this study, such relaxors can be found in the matrix farther from the filler interfaces, where the local environments are identical in all systems studied. In contrast, the interfacial modes, in addition to their distinct dynamics, were also characterized by different activation energies, ΔE_A, whose values depend on the filler phase: Namely, for the oMMT composites in Fig. 7, ΔE_A is approximately 105 kJ/mol, whereas for the 30 vol % BT composite it is 51 kJ/mol. This significant decrease in the energy barriers associated to

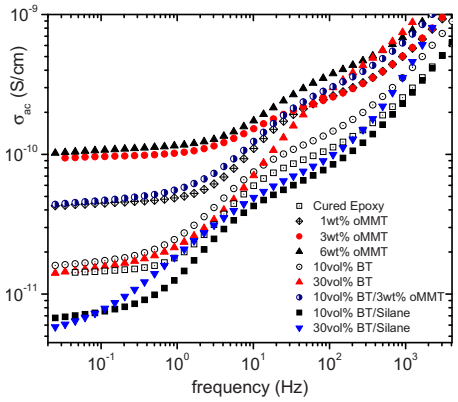

FIG. 8. (Color online) Comparative ac conductivity curves for all investigated systems at 160 °C.

the interfacial relaxation processes clearly manifest weaker interactions between the BT fillers and the epoxy network, compared to the epoxy/oMMT interfaces, and this relative strength of interfacial interactions is also in concert with the corresponding faster relaxation dynamics discussed previously.

C. DRS at temperatures above T_g

1. Conductivity studies

Dielectric measurements were also performed at temperatures higher than the glass transition temperature of the samples, in order to investigate the space charge conduction processes present in the system.[32,61–64] Figure 8 illustrates the frequency dependence of the ac conductivity, $\sigma_{ac}(f)$, for all the systems at 160 °C. In the low frequency limit, the frequency independent plateau value of σ_{ac} indicates the dc conductivity (σ_{dc}). A correlation between the filler type and concentration and the σ_{dc} value is evident: Compared to the unfilled epoxy, σ_{dc} increases by almost one order of magnitude for the 3 wt % oMMT composites (increasing the filler loading to 6 wt % does not generate further increase in conductivity, which indicates that the corresponding percolation threshold was already reached prior to 6 wt %). In contrast, the BT composites do not show a significant change in σ_{dc}, not even at the highest filler concentrations studied. Furthermore, silane modification of the BT causes the composites' conductivity to decrease approximately by half a decade in both 10 and 30 vol % loadings in silanated-BT. Interestingly, in the dual-filler composites σ_{dc} falls between the dc values of the corresponding single-filler composites, despite the phase separated morphology and the substantially less-dispersed oMMT in the dual-filler systems.

In order to further clarify the filler effect on the dc conductivity, the conduction process was investigated in the temperature range between T_g and 180 °C (the postcuring temperature). Figure 9 presents the Arrhenius plots for the measured dc conductivities of all systems. The activation energies of the dc conductivity processes were calculated from the best linear fits of Eq. (5) to the experimental data and are summarized in Table III.

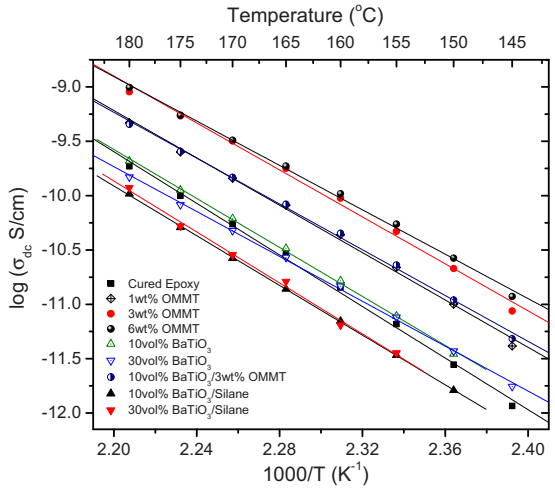

FIG. 9. (Color online) Arrhenius plot of the dc conductivity for all systems studied. The values were obtained at 0.04 Hz and the temperature range is between the corresponding glass transition and the post curing temperatures.

$$\sigma_{dc}(T) = \sigma_0 \exp\left(-\frac{\Delta E_A}{k_B T}\right). \quad (5)$$

The σ_{dc} activation energy follows a similar trend as the one observed for the T_g data. Specifically, the unfilled epoxy matrix shows the highest activation energy and ΔE_A systematically decreases with increasing filler concentration, with the decrease being more prominent in the oMMT composites. Taking into account the IR results, this behavior further strengthens the supposition that an uncrosslinked polymer phase is present in the vicinity of the filler surfaces. This phase exhibits higher mobility compared to that in the crosslinked phase and therefore is expected to enhance the conduction process. The validity of this supposition is supported by both the magnitude of the dc conductivities and by the corresponding lower ΔE_A values, especially evident with higher filler loadings in oMMT and BT. These values further suggest that the relevant percolation threshold of the two filler phases to be around 30 vol % for BT and 6 wt % for oMMT. The activation energies, within the errors, were found to be the same for the two fillers (measurements at higher filler concentrations, to further confirm that the ΔE_A values reached a plateau, could not be performed due to dispersion difficulties in the composite preparation). Interest-

TABLE III. Activation energies of the dc conductivity process obtained from the linear fit of Eq. (2) to the experimental data in Fig. 9.

Sample	ΔE_A (kJ/mol)	ΔE_A (eV)
Epoxy matrix	227 ± 5	2.35 ± 0.05
1 wt % oMMT	209 ± 5	2.17 ± 0.05
3 wt % oMMT	207 ± 6	2.15 ± 0.06
6 wt % oMMT	196 ± 4	2.03 ± 0.04
10 vol % $BaTiO_3$	216 ± 3	2.24 ± 0.03
10 vol % $BaTiO_3$/silane	219 ± 2	2.27 ± 0.02
10 vol % $BaTiO_3$/3 wt % oMMT	202 ± 4	2.09 ± 0.04
30 vol % $BaTiO_3$	198 ± 3	2.05 ± 0.03
30 vol % $BaTiO_3$/silane	225 ± 7	2.33 ± 0.07

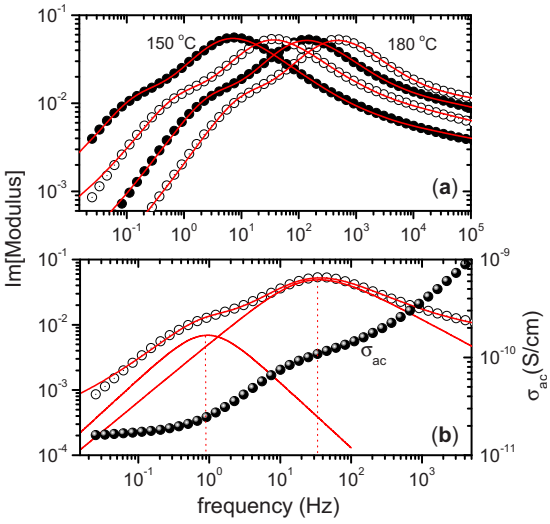

FIG. 10. (Color online) (a) The imaginary part of the electric modulus for the 10 vol % $BaTiO_3$ composite along with the fitting curves. The presented temperature interval is from 180 to 150 °C in steps of 10 °C. (b) Analysis of the 160 °C spectrum, including the corresponding conductivity plot (solid spheres); the low frequency contribution corresponds to the onset of dc conductivity, whereas the high frequency contribution corresponds to the MWS space-charge relaxation.

ingly, BT silane modification compensated the decrease in activation energy for the 30 vol % BT composite (as shown in Table III, the improvement of the interface leads to a significant increase in the ΔE_A value); however, the absolute value of σ_{dc} also depends on the glass transition temperature and the space-charge dynamics, *vide infra* Sec. III C 2.

2. Space-charge studies

In Fig. 8 a relaxation in the $\sigma_{ac}(f)$ conductivity function can be observed at higher frequencies. In this region, conductivity is frequency dependent and describes the short range motions of the space-charge carriers, i.e., a subdiffusive type of transport due to sublinear dependence of the mean square displacement on time.[65,66] For the short time scales probed by DRS, the charges are confined at the boundaries between regions with different conductivities and permittivities.[67] The space-charge interfacial dynamics [Maxwell–Wagner–Sillars (MWS) relaxation[68–70]] are different in the various composites, and, evidently, depend on the dielectric properties and geometry of the filler/phases in the composites; therefore, analysis of this relaxation can provide information regarding the effect of fillers on the dc conductivity process. The $M^*(\omega)$ modulus formalism can be utilized here to illustrate the weak relaxation contributions, that are usually masked by conductivity effects in the permittivity $\epsilon^*(\omega)$ formalism.[71] Figure 10(a) shows the imaginary part $M''(\omega)$ of the 10 vol % $BaTiO_3$ composite for selected temperatures (180 to 150 °C). Two relaxation processes contribute to the spectrum, and both these processes shift to higher frequencies with increasing temperature. Appropriate expressions resolving the imaginary and real part of the electric modulus are well-established in the literature.[72,73] The frequency of the low-frequency peak maximum corresponds to the onset of dc conductivity, as shown in Fig. 10(b), and therefore this mode is attributed to the conductivity relaxation (in further support of this, the corresponding Arrhenius plot (not shown) was found to have the same dependence on the filler type and loading as the σ_{dc} Arrhenius plot in Fig. 9). The broad mode at higher frequencies relates to the space charge interfacial relaxation, MWS, and can clearly be observed in Fig. 10(b). The best fitting to the experimental data was obtained by a Havriliak–Negami expression (which reduces to the Debye equation for $\alpha=1-\beta=0$) superimposed to the low frequency Debye process:[72,73]

$$M'(\omega) = M_\infty M_s \times \frac{[M_s A^\beta + (M_\infty - M_s)\cos\beta\phi]A^\beta}{M_s^2 A^{2\beta} + 2A^\beta (M_\infty - M_s)M_s \cos\beta\phi + (M_\infty - M_s)^2}, \tag{6}$$

$$M''(\omega) = M_\infty M_s \times \frac{[(M_\infty - M_s)\sin\beta\phi]A^\beta}{M_s^2 A^{2\beta} + 2A^\beta (M_\infty - M_s)M_s \cos\beta\phi + (M_\infty - M_s)^2}, \tag{7}$$

where

$$A = [1 + 2(\omega\tau_o)^{1-\alpha}\sin(\alpha\pi/2) + (\omega\tau_o)^{2(1-\alpha)}]^{1/2}, \tag{8}$$

and

$$\phi = \arctan\left[\frac{(\omega\tau_o)^{1-\alpha}\cos(\alpha\pi/2)}{1 + (\omega\tau_o)^{1-\alpha}\sin(\alpha\pi/2)}\right],$$
$$\omega_{\max}\tau_o = \tan\left(\frac{1}{\beta+1}\frac{\pi}{2}\right). \tag{9}$$

An Arrhenius plot reveals that the slowest space-charge MWS dynamics correspond to the silane modified BT composites and the fastest to the 6 wt % oMMT systems. As expected, this trend is in good agreement with the variation in the dc conductivity values (Figs. 8 and 9) since both phenomena share a common physical origin. Namely, both σ_{dc} and the interfacial MWS dynamics are due to the mobility of the catalyst residues in the epoxy: these ionic residues (termed as space-charge because they are impurities) are trapped within the epoxy network or at the organic/inorganic interfaces and give rise to MWS relaxations at short time scales; at longer time scales, these same charges have sufficient time to escape from their traps and diffuse giving rise to a dc conductivity. Upon surface modification, the accumulated charges at the silanated-BT interfaces exhibit retardation in their dynamics, compared to the corresponding dynamics of the composites with unmodified BT fillers. This behavior relates to the space-charge interactions with the polar groups of the silanes that are grafted on the BT filler surfaces and, based on these data, they appear to be less mobile. The slow down in the MWS dynamics will necessitate longer time scale for the onset of dc conductivity and will consequently decrease the corresponding conductivity plateau value. In contrast, the faster dynamics in the 6 wt % oMMT composite reflect the high interfacial area effect on the space-charge mobility. As observed before, cf. Fig. 3, increasing the interfacial area leads to the formation of uncrosslinked/mobile regions, which should also promote the

enhancement of the space-charge mobility accordingly.

Due to their nature, the space-charge dynamics are intrinsically related to the variation in T_g (shown in Fig. 2 and Table I). At temperatures higher than T_g, the dynamics of the polymer network become faster with increasing temperature, and in order to separate any interfacial effects, the Arrhenius plot is normalized by the respective T_g of each composite.[74] Such an analysis, still shows that the space charge dynamics of the 30 vol % silane-BT and of the 6 wt % oMMT composites correspond to the slowest and the fastest dynamics, respectively. This behavior indicates the dominance of the interfacial effect over the glass transition effect on the dynamics of the space-charge. The other composites studied, especially those with lower contents of various fillers, do not exhibit a systematic variation in their dynamics when normalized by their T_g. Most probably, the lack of a systematic trend here reflects the differences in dispersion (the space-charge dynamics/conductivity depend on filler area, on crosslinking density next to the inorganic particles, and on the polymer-filler interactions, all of which are determined by filler dispersion[75]).

D. Dielectric properties under high electric field

1. Dielectric breakdown strength

Beyond the low electric field relaxations, the epoxy nanocomposites of this work were also investigated for their high field performance through a series of dielectric breakdown tests. The characteristic electric breakdown strength of the composites is analyzed within the frame of Weibull statistics, using a mean sample size of 15 to calculate the Weibull parameters from the cumulative probability of failure P, through $P=1-\exp[-(E_{BD}/\alpha_w)^{\beta_w}]$ (α_w is the statistical estimator of the breakdown strength E_{BD}, corresponding to a cumulative probability of failure equal to $1-e^{-1}$, with a scattering in the data reducing as β_w increases[53]). Figure 11 shows the dielectric strengths of all composites, i.e., of the single filler epoxy/BT and epoxy/oMMT, and of the dual-filler epoxy/BT/oMMT composites, as quantified by the Weibull α_w parameter. There exists a systematic decrease in the characteristic breakdown strength of epoxy/$BaTiO_3$ composites with increasing content of $BaTiO_3$. This result is easily understood by simply considering the field enhancement at the interface of the high permittivity BT filler, which is encapsulated inside a much lower permittivity epoxy matrix: As the concentration of the BT filler increases, the average interparticle distance decreases, and consequently the electric field concentration at the polymer-filler interfaces is amplified; this creates more points of initiation of local breakdown channels (i.e., creating a divergent field that may propagate the breakdown channel through the *local* weakest links). On the contrary, at large concentration of high permittivity fillers the field distribution inside the composites becomes more uniform.[76–78] Consequently, the breakdown channels become predominately defect dominated and propagate through the *global* weakest link present in a quasi-homogenous field, leading to a leveling of the breakdown-down strength values.[79]

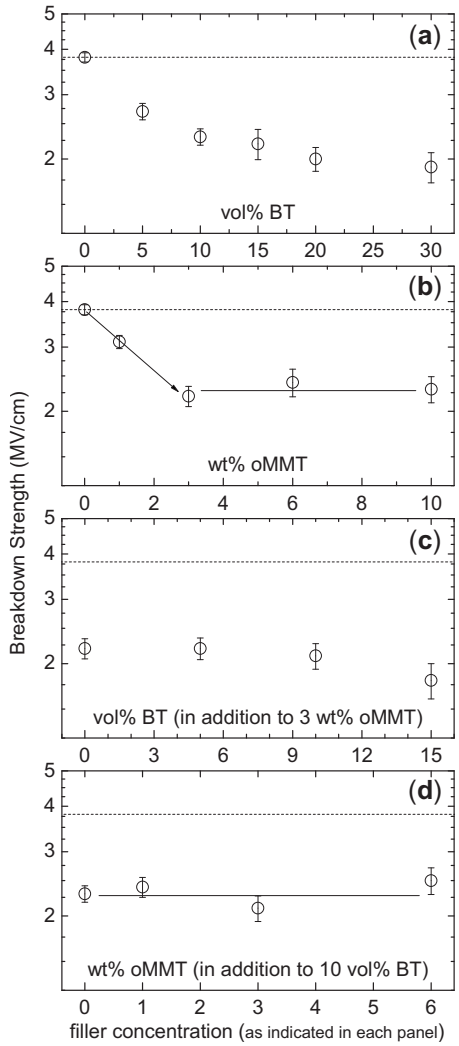

FIG. 11. Dielectric breakdown strength (Weibull α_w parameter) of epoxy nanocomposites as a function of filler loading: (a) epoxy/$BaTiO_3$ composites; (b) epoxy/oMMT composites; (c) dual-filler composites with 3 wt % oMMT (fixed) plus varying volume percent of $BaTiO_3$ (referred as T-1) (d) dual-filler composites with 10 vol % of $BaTiO_3$ (fixed) plus varying weight percent of oMMT (referred as T-2). The dashed lines depict the breakdown strength of the unfilled cured epoxy, the solid lines are drawn as a guide to the eye. All Weibull β_w values range between 5 and 8, except for the unfilled epoxy and the dual-filler 10 vol % BT/6 wt % oMMT composite where β_w is larger than 8.

Nanocomposites filled with large aspect ratio fillers can be very beneficial because they contain large interfacial areas, which, if properly designed, could promote interfacial exchange coupling through a dipolar interface layer and lead to enhanced polarization/polarizability.[54,80–82] Also, fillers such as oMMT provide low or none dielectric mismatch between the filler and matrix and, thus, are not expected to introduce problems associated with local field enhancements at the polymer-filler interfaces. However, our results showed that the epoxy/oMMT nanocomposites breakdown strength also decreased, even at the lowest concentrations used. in fact, the drop in dielectric strength is sharp at the lowest oMMT concentrations and tends to level-off after 3 wt % oMMT loadings. The initial decrease in breakdown strength with oMMT can be accounted for by the higher ionic conductivity of these composites and the higher concentration of

unreacted epoxy units present (discussed above), as compared to $BaTiO_3$ filled composites. Whereas, the leveling off at higher loadings of oMMT indicates the onset of percolation of the interfacial regions, and demonstrates the significant role of filler dispersion in determining the dielectric strength. Beyond the percolation, the breakdown strength may rebound and can be associated to the reduced field fluctuation present inside highly-filled nanocomposites. However, in contrast to high BT loadings, in the case of oMMT it is much more difficult to make any reasonable predictions for the breakdown strength beyond the percolation, since at such high oMMT concentrations there exist multiple competing mechanisms that can influence the breakdown behavior.

Dual-filler composites with varying concentrations of both fillers were also investigated to evaluate any synergistic or emergent benefits of simultaneously adding high permittivity BT and high aspect ratio oMMT fillers. Figures 11(c) and 11(d) depict the high field behavior of several dual-filler composites. An apparent degradation in the breakdown strength is again evident in both fixed-concentration $BaTiO_3$ (referred as T-1) and fixed-concentration oMMT (referred as T-2) phase separated (nano)composites, when the concentration of the second type filler is varied. In more detail, there is a systematic decrease in performance of the T-1 systems with higher volume percent of $BaTiO_3$ at a constant 3 wt % oMMT, very similar to that observed in epoxy/BT composites. Interestingly, increasing the oMMT concentrations in T-2 composites, at a constant 10 vol % of $BaTiO_3$, showed no marked change in the breakdown strength value, which remained close to the plateau value of the epoxy/oMMT composites for all T-2 systems. The scattering in the breakdown strengths, as shown in Fig. 11(d), is probably due to oMMT dispersion differences, which can also be accompanied by differences in the concentration of uncured epoxy species, as indicated by Fig. 3. Hence, for making composites with improved breakdown strength it is imperative to better design the nanocomposite systems toward: (a) removing the phase separation of BT and oMMT fillers, and (b) designing stronger filler-epoxy interfaces. Both these are addressed in the follow-up paper.[53] However, such design approaches necessitate a better understanding of the effect of uncured epoxy species on the high field electrical properties and on the composites' breakdown strength.

2. Dielectric strength dependence on extend of crosslinking

The presence of fillers causes an increase in the fraction of unreacted epoxy in these nanocomposites, as clearly observed in Fig. 3. This also results in lowering the corresponding glass transition temperatures of the nanocomposites, an effect which impacts negatively their mechanical properties. In order to quantify the effect of incomplete crosslinking on the electrical properties, we prepared *unfilled* epoxy samples and varied their curing time. In Fig. 12, we plot the obtained values for their glass transition temperatures and their corresponding dielectric breakdown strength, for unfilled epoxies as a function of curing time. As expected, a systematic increase in the glass transition temperature is observed with increasing time of cure. At the same time, the dielectric

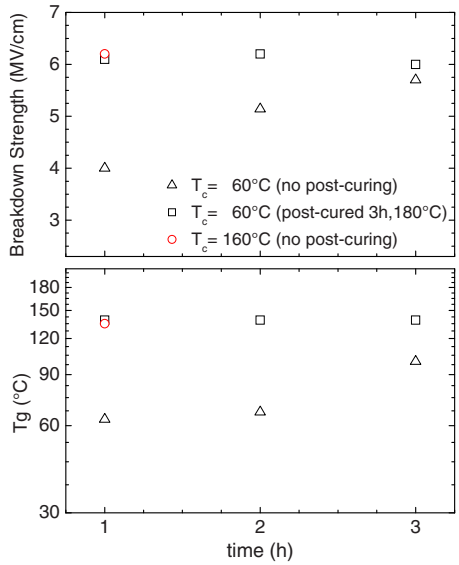

FIG. 12. (Color online) Characteristic breakdown strength (Weibull α_w) and glass transition temperature (calorimetric T_g) for an *unfilled* epoxy as a function of curing time. Epoxies were cured at 60 °C for the indicated time, and were either tested as such (triangles) or after postcuring at 180 °C for three additional hours (squares); for comparison an epoxy cured at 160 °C is also shown (circle). The trends of T_g and breakdown strength are very similar.

breakdown strength also increased with increasing time of cure, suggesting a correlation with the crosslinking density of the thermoset polymer matrix. Displacement-electric-field (*D-E*) loops shown in Fig. 13(a) further confirm the same trend in the dielectric properties of unfilled epoxy with cure time, that is, with the percentage of crosslinking, as is evidenced by the systematic decrease in the *D-E* slopes (the *D-E* slope defines the permittivity under high electric field). Similar results are obtained from varying the concentration of curative present in the system [Fig. 13(b), or in more detail elsewhere[53]]. The breakdown strength (Weibull strength and modulus, α_w and β_w) also depends on the extend of crosslinking in a similar manner, cf. Figs. 12 and 13(b).

These observations from the unfilled epoxies provide direct insights in the origins of the observed loss in dielectric strength in the composites: Specifically, for the oMMT nanocomposites there exist extensive organic–inorganic interfaces, even at moderate dispersion or low filler loading, which promote uncrosslinked epoxide groups, which, in turn, lower the dielectric strength of the composites. These results further signify the importance of designing these polymer-filler interfaces, which should maintain proper crosslinking density in the nanocomposites, if one wants to capitalize on such filler to achieve improved dielectric strengths. Given the nature of these inorganic nanoparticulates, this can only be done by introducing reactive groups on the oMMT surfaces that can participate in the crosslinking of the epoxy, as is discussed in detail in the second paper of this series.[53] From this starting point, the electric properties of nanocomposites with spherical [three-dimensional (3D)], platelet [two-dimensional (2D)], and simultaneous 3D and 2D nano-

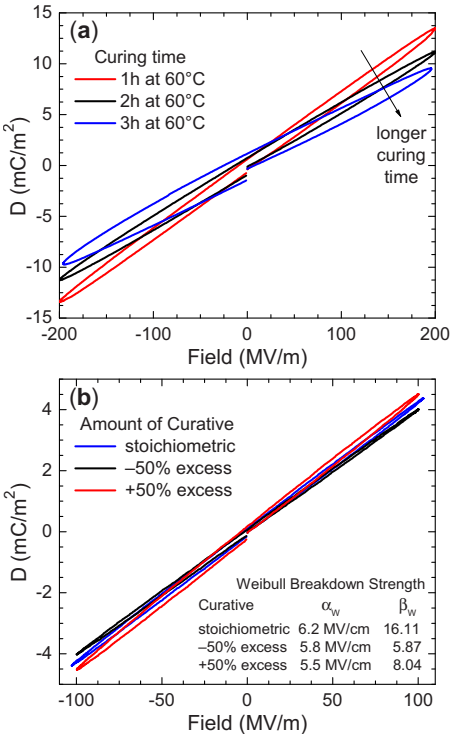

FIG. 13. (Color online) *D-E* loops for *unfilled* epoxies, highlighting the effect of extend of crosslinking on the high field dielectric properties. (a) The dependence on curing time reveals a marked improvement in high field performance with higher crosslinking density. (b) The dependence on curative concentration also shows improvement with better crosslinking, albeit less pronounced than in (a), whereas the respective breakdown strengths (inset) show a marked systematic improvement.

fillers, can be improved by proper choice of the inorganic fillers and thus enable high-performance materials for electric storage.[53]

3. Recoverable energy density

Fillers with high permittivity create dielectric inhomogeneities at the polymer-filler interfaces within the composite and, in the case of nanometer-scale fillers, these interfaces can dictate the macroscopic behavior of the material.[11,12,53] In particular, as demonstrated in the previous sections, these interfaces play a central role in controlling the ac and dc conductivities and the space-charge formation and relaxation, and thus they are also expected to determine the dielectric breakdown strengths. This line of thought naturally leads one to expect that the recoverable energy densities of these composites would change accordingly. Toward checking this hypothesis, *D-E* loops were obtained, in order to quantify and understand the behavior of recoverable energy density in these composites. The widening (or opening) of the *D-E* loops depicts a deviation from the linear behavior of the dielectric displacement versus the electric field ($D=\varepsilon_0\varepsilon' E=\varepsilon_0 E+P$, where P is the polarization) and is related to the losses (space-charge, conduction, etc.) present in the system. We present comparative results for the unfilled epoxy, the epoxy/BT and epoxy/oMMT nanocomposites, as well as for the dual-filler systems. The expected linear behavior of the dielectric displacement with the applied field is observed for the unfilled epoxy system. Upon nanofiller addition, the calculated area inside the *D-E* loops increased as a function of applied field, for all composites. In particular, the widening of the displacement-field loops is more pronounced in those composites containing high permittivity $BaTiO_3$ fillers, emphasizing that the magnitude of losses is related to the organic-inorganic permittivity contrast. Accordingly, the epoxy/oMMT nanocomposites show comparably smaller losses than the epoxy/BT system, as expected from the smaller matrix-filler permittivity difference in this case. The recoverable energy density as a function of applied field is presented in Fig. 14. It is clearly evident, cf. Figs. 14(b) and 14(d), that the low permittivity oMMT filler does not enhance the recoverable energy densities; namely, irrespective of oMMT filler concentration the (nano)composites do not show any marked change in recoverable energy density. In contrast, the epoxy/BT composites demonstrated increasing values in their recoverable energy densities, especially with higher applied field [Fig. 14(a)]. Regardless of any difference in the losses present, the enhancement in recoverable energy density is found to correlate well with the concentration of $BaTiO_3$. Finally, in accord with this last trend, the epoxy/BT/oMMT dual-filler composites also exhibit improvement in energy density with increasing $BaTiO_3$ [Fig. 14(c)]. These results further exemplify the importance of introducing high permittivity fillers in improving the energy storage performance of these composites.

IV. CONCLUSIONS

Epoxy/inorganic nanocomposite systems display some advantageous dielectric behaviors at low nanofiller loadings. In this work we systematically varied the filler loading and type, incorporating nanoscale BT, oMMT, and a combination of both these nanoparticulates in a crosslinkable epoxy matrix. Studies of the resulted (nano)composites recorded changes in the crosslinking density, the glass transition, and the interfacial polymer dynamics, which were subsequently correlated with the respective dielectric responses. For such nanocomposites, high permittivity BT fillers resulted in increased permittivity and loss values, compared to the respective unfilled systems, whereas addition of lower permittivity oMMT did not have a marked effect.

For all (nano)composites, a significant change in the local environment of the polymer was found after the incorporation of nanofillers. This change was primarily traced in increased populations of uncrosslinked epoxide groups near the filler interfaces, accompanied by an associated reduction in the T_g values. Further dielectric spectroscopy studies revealed new dynamics and unique conductivity characteristics in the nanocomposites, which follow the same trends as their respective glass transition temperatures. Specifically, dielectric spectroscopy identified two different types of relaxations, the bulk response of the cured epoxy matrix and a new, higher activation energy, and slower relaxation response, which was characteristic of the nanofiller type. This indicates that different fillers create different types of interfaces and interfacial dynamics, which macroscopically manifest in differences in space-charge development and in high electric field responses. The addition of silanes on the BT particles

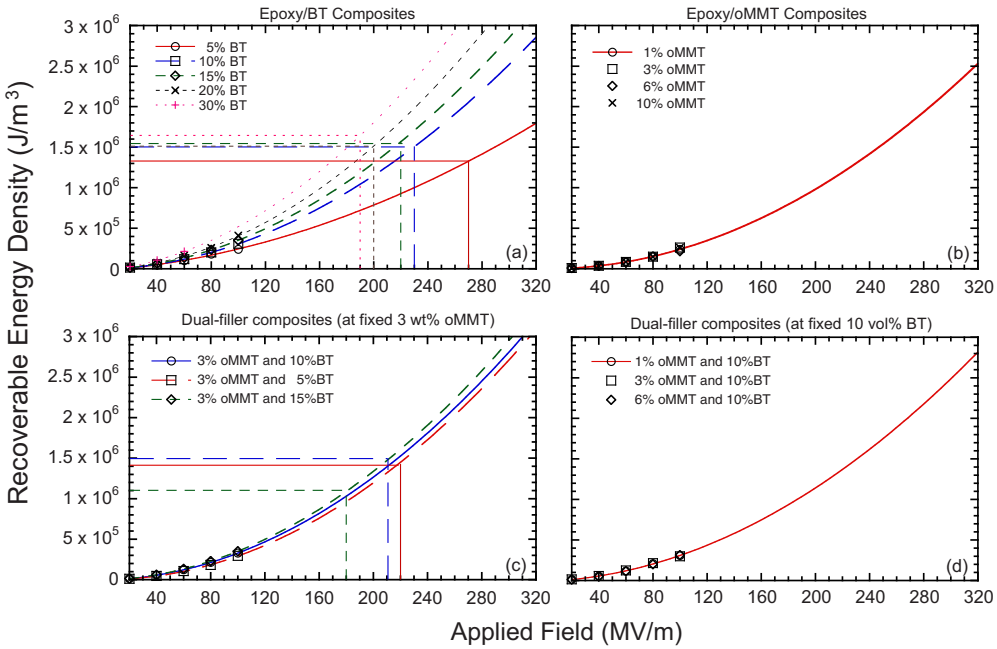

FIG. 14. (Color online) Recoverable energy density of epoxy composites as a function of applied field. (a) epoxy/$BaTiO_3$ nanocomposites; (b) epoxy/oMMT nanocomposites; (c) dual-filler epoxy/BT/oMMT composites at a fixed 3 wt % oMMT loading with varying $BaTiO_3$ concentration; and (d) dual-filler epoxy/BT/oMMT composites at a fixed 10 vol % $BaTiO_3$ and varying oMMT concentration. The energy densities have been extrapolated assuming a monotonic increase in the losses up to the breakdown field levels (the validity of linearity was experimentally confirmed), and intercepts are drawn at the observed dc breakdown fields.

improved the interfacial contact, and enhanced the performance of these composites with respect to their energy storage capability. A reduction in the epoxy dc volume resistivity was also observed upon nanofiller incorporation and, more notably, although the dc dielectric strengths of all nanocomposites were lower than those of unfilled epoxy systems, there were distinct benefits in their recoverable energy density values: Specifically, BT nanofillers resulted in increased recoverable energy densities, while no advantages were found for oMMT fillers. This demonstrates that high permittivity fillers are indeed crucial in enhancing the energy storage capabilities of low permittivity polymers, such as epoxies, however, attention must be paid to improve the matrix-filler interfaces, so as not to sacrifice other materials properties.

ACKNOWLEDGMENTS

This work was supported by the Office of Naval Research (Grant No. MURI-00014-05-1-0541). G.P. and E.M. acknowledge additional financial support by the National Science Foundation (NSF) (Grant No. DMR-0602877).

[1]J. P. Calame, in *Conference Record of the 2006 IEEE International Symposium on Electrical Insulation*, Toronto, Ontario, Canada, 11–14 June 2006 (IEEE, New York, 2006), p. 466–469.
[2]I. Burn and D. M. Smyth, J. Mater. Sci. **7**, 339 (1972).
[3]G. R. Love, J. Am. Ceram. Soc. **73**, 323 (1990).
[4]F. MacDougall, J. Ennis, R. Cooper, J. Bates, and K. Seal, in *14th IEEE International Pulsed Power Conference, Digest of Technical Papers*, San Diego, CA, 15–18 June 2003, (IEEE, New York, 2008), Vol. 1, p. 513.
[5]M. Rabuffi and G. Picci, IEEE Trans. Plasma Sci. **30**, 1939 (2002).
[6]G. Blaise and W. J. Sarjeant, IEEE Trans. Dielectr. Electr. Insul. **5**, 779 (1998).
[7]F. Hussain, J. H. Chen, and M. Hojjati, Mater. Sci. Eng., A **445–446**, 467 (2007).
[8]T. Tanaka, IEEE Trans. Dielectr. Electr. Insul. **12**, 914 (2005).
[9]T. Tanaka, G. C. Montanari, and R. Mulhaupt, IEEE Trans. Dielectr. Electr. Insul. **11**, 763 (2004).
[10]V. Tomer, J. Kostelnick, G. Polizos, E. Manias, and C. A. Randall, in *17th IEEE International Symposium on the Applications of Ferroelectrics*, Santa Fe, New Mexico, 23–28 February 2008 (IEEE, New York, 2008), Vol. 2, p. 1.
[11]V. Tomer, C. Randall, G. Polizos, and J. Kostelnick, J. Appl. Phys. **103**, 034115 (2008).
[12]V. Tomer and C. A. Randall, J. Appl. Phys. **104**, 074106 (2008).
[13]E. Manias, Nature Mater. **6**, 9 (2007).
[14]C. Chen and D. Curliss, Nanotechnology **14**, 643 (2003).
[15]C. Chen and T. B. Tolle, J. Polym. Sci., Part B: Polym. Phys. **42**, 3981 (2004).
[16]H. Miyagawa, L. T. Drzal, and J. A. Carsello, Polym. Eng. Sci. **46**, 452 (2006).
[17]H. Miyagawa, M. J. Rich, and L. T. Drzal, J. Polym. Sci., Part B: Polym. Phys. **42**, 4384 (2004).
[18]F. Hussain, M. Hojjati, M. Okamoto, and R. E. Gorga, Journal Of Composite Materials **40**, 1511 (2006).
[19]T. Iizuka, K. Uchida, and T. Tanaka, in *Conference on CEIDP 2007 Annual Report*, Vancouver, BC, Canada (2007) (IEEE, New York, 2007), p. 236.
[20]P. Preetha, S. Alapati, S. Singha, B. Venkatesulu, and M. J. Thomas, in *Conference on CEIDP 2008 Annual Report*, Quebec, QC, Canada (2008) (IEEE, New York, 2008), p. 718.
[21]N. Salahuddin, A. Moet, A. Hiltner, and E. Baer, Eur. Polym. J. **38**, 1477 (2002).
[22]R. Sarathi, R. K. Sahu, and P. Rajeshkumar, Mater. Sci. Eng., A **445–446**, 567 (2007).
[23]S. Singha and M. J. Thomas, IEEE Trans. Dielectr. Electr. Insul. **15**, 12 (2008).
[24]Y. Sun, Z. Zhang, K. Moon, and C. Wong, J. Polym. Sci., Part B: Polym. Phys. **42**, 3849 (2004).
[25]N. Tagami, M. Okada, N. Hirai, Y. Ohki, T. Tanaka, T. Imai, M. Harada, and M. Ochi, IEEE Trans. Dielectr. Electr. Insul. **15**, 24 (2008).
[26]W. Xu, P. He, and D. Chen, Eur. Polym. J. **39**, 617 (2003).
[27]J. C. Fothergill, J. K. Nelson, and M. Fu, in *Conference on CEIDP 2004 Annual Report*, 17–20 October 2004 (IEEE, New York, 2004), p. 406.
[28]E. Tuncer, I. Sauers, D. R. James, A. R. Ellis, M. P. Paranthaman, T. Aytug, S. Sathyamurthy, K. L. More, J. Li, and A. Goyal, Nanotechnology

18, 025703 (2007).
[29]J. A. Forrest, K. Dalnoki-Veress, and J. R. Dutcher, Phys. Rev. E **56**, 5705 (1997).
[30]H. Oh and P. Green, Nature Mater. **8**, 139 (2009); G. Polizos, E. Tuncer, I. Sauers, and K. L. More, Appl. Phys. Lett. **96**, 152903 (2010).
[31]F. Starr, T. Schroder, and S. Glotzer, Phys. Rev. E **64**, 021802 (2001); S. H. Anastasiadis, K. Karatasos, G. Vlachos, E. Manias, and E. P. Giannelis, Phys. Rev. Lett. **84**, 915 (2000).
[32]J. K. Nelson and J. C. Fothergill, Nanotechnology **15**, 586 (2004).
[33]J. K. Nelson and Y. Hu, IEEE International Conference on Solid Dielectrics, ETATS-UNIS, Toulouse, France, 2004, p. 832.
[34]R. C. Smith, C. Liang, M. Landry, J. K. Nelson, and L. S. Schadler, IEEE Trans. Dielectr. Electr. Insul. **15**, 187 (2008).
[35]M. Kozako, S. Yamano, R. Kido, Y. Ohki, M. Kohtoh, S. Okabe, and T. Tanaka, *Preparation and Preliminary Characteristic Evaluation of Epoxy/Alumina Nanocomposites*, Proceedings of 2005 International Symposium on Electrical Insulating Materials, Kitakyushu, Japan, 5–9 June 2005 (IEEE, New York, 2005), Vol. 1, p. 231–234.
[36]L. Ramajo, M. S. Castro, and M. M. Reboredo, Composites, Part A **38**, 1852 (2007).
[37]T. J. Lewis, J. Phys. D: Appl. Phys. **38**, 202 (2005).
[38]G. Picci and M. Rabuffi, in *Conference Record of the 2001 IEEE Pulsed Power Plasma Science*, Las Vegas, Nevada (2001) (IEEE, New York, 2001), p. 374.
[39]R. Picu and M. Ozmusul, J. Chem. Phys. **118**, 11239 (2003).
[40]T. Tanaka, M. Kozako, N. Fuse, and Y. Ohki, IEEE Trans. Dielectr. Electr. Insul. **12**, 669 (2005).
[41]D. B. Zax, D. K. Yang, R. A. Santos, H. Hegemann, E. P. Giannelis, and E. Manias, J. Chem. Phys. **112**, 2945 (2000).
[42]E. Manias, G. Hadziioannou, and G. ten Brinke, J. Chem. Phys. **101**, 1721 (1994).
[43]E. Manias, V. Kuppa, D. K. Yang, and D. B. Zax, Colloids Surf., A **187–188**, 509 (2001).
[44]V. Kuppa, T. M. D. Foley, and E. Manias, Eur. Phys. J. E **12**, 159 (2003).
[45]E. Manias and V. Kuppa, Eur. Phys. J. E **8**, 193 (2002).
[46]S. Liang, S. R. Chong, and E. P. Giannelis, in *Conference of the 48th IEEE Electronic Components and Technology*, Seattle, Washington, 25–28 May (1998) (IEEE, New York, 1998), p. 171–175.
[47]S. Ramesh, B. A. Shutzberg, C. Huang, J. Gao, and E. P. Giannelis, IEEE Trans. Adv. Packag. **26**, 17 (2003).
[48]Z. Lu, G. Polizos, D. D. Macdonald, and E. Manias, J. Electrochem. Soc. **155**, B163 (2008); Z. Lu, M. Lanagan, E. Manias, and D. D. Macdonald, J. Phys. Chem. B **113**, 13551 (2009).
[49]A. F. Koster van Groos and S. Guggenheim, Am. Mineral. **74**, 627 (1989).
[50]R. A. Vaia and E. P. Giannelis, Macromolecules **30**, 8000 (1997).
[51]E. Manias, J. Zhang, J. Y. Huh, K. Manokruang, P. Songtipya, and M. M. Jimenez-Gasco, Macromol. Rapid Commun. **30**, 17 (2009).
[52]R. E. Newnham, Ferroelectrics **68**, 1 (1986).
[53]G. Polizos, V. Tomer, E. Manias, and C. A. Randall, J. Appl. Phys. **108**, 074117 (2010).
[54]L. Wu, S. V. Hoa, M. Tan, and T. That, J. Appl. Polym. Sci. **99**, 580 (2006).
[55]A. T. Chien, X. Xu, J. H. Kim, J. Sachleben, J. S. Speck, and F. F. Lange, J. Mater. Res. **14**, 3330 (1999).
[56]S. Lee, C. A. Randall, and Z. K. Liu, J. Am. Ceram. Soc. **92**, 222 (2009).
[57]B. Lestriez, A. Maazouz, J. F. Gerard, H. Sautereau, G. Boiteux, G. Seytre, and D. E. Kranbuehl, Polymer **39**, 6733 (1998).
[58]F. Kremer and A. Schönhals, *Broadband Dielectric Spectroscopy* (Springer, Berlin, 2003).
[59]N. G. McCrum, B. E. Read, and G. Williams, *Anelastic and Dielectric Effects in Polymeric Solids* (Wiley, New York, 1967).
[60]J. Mijović and H. Zhang, Macromolecules **36**, 1279 (2003).
[61]J. D. Jacobs, H. Koerner, H. Heinz, B. L. Farmer, P. Mirau, P. H. Garrett, and R. A. Vaia, J. Phys. Chem. B **110**, 20143 (2006).
[62]T. Cajkovski, M. Davidovic, P. Pissis, G. Polizos, D. Cajkovski, V. Likar-Smiljanic, R. Biljic, Z. Nedic, and U. B. Mioc, Solid State Ionics **162–163**, 203 (2003).
[63]S. D. Senturia and N. F. Sheppard, Adv. Polym. Sci. **80**, 1 (1986).
[64]N. F. Sheppard and S. D. Senturia, J. Polym. Sci., Part B: Polym. Phys. **27**, 753 (1989).
[65]K. Funke, B. Roling, and M. Lange, Solid State Ionics **105**, 195 (1998).
[66]B. Roling, C. Martiny, and K. Funke, J. Non-Cryst. Solids **249**, 201 (1999).
[67]K. Yamamoto and H. Namikawa, Jpn. J. Appl. Phys., Part 1 **27**, 1845 (1988).
[68]J. C. Maxwell, *Electricity and Magnetism*, 4th ed. (Clarendon, Oxford, 1892), Vol. 1.
[69]R. W. Sillars, J. Inst. Electr. Eng. **80**, 378 (1937).
[70]K. W. Wagner, Arch. Elektrotech. (Berlin) **9**, 371 (1914).
[71]A. G. Charnetskaya, G. Polizos, V. I. Shtompel, E. G. Privalko, Y. Y. Kercha, and P. Pissis, Eur. Polym. J. **39**, 2167 (2003).
[72]G. C. Psarras, E. Manolakaki, and G. M. Tsangaris, Composites, Part A **33**, 375 (2002).
[73]G. M. Tsangaris, G. C. Psarras, and N. Kouloumbi, J. Mater. Sci. **33**, 2027 (1998).
[74]G. Polizos, V. V. Shilov, and P. Pissis, J. Non-Cryst. Solids **305**, 212 (2002); Solid State Ionics **145**, 93 (2001).
[75]J. Zhang, E. Manias, and C. A. Wilkie, J. Nanosci. Nanotechnol. **8**, 1597 (2008).
[76]S. Boggs and K. Jinbo, IEEE Electr. Insul. Mag. (USA) **14**, 5 (1998).
[77]J. Calame, *Microstructure-Based Simulation of the Dielectric Properties of Polymer-Ceramic Composites for Capacitor Applications, Smart Dielectric Polymer Properties, Characterization and Their Devices*, edited by V. Bharti, Z. Cheng, Q. M. Zhang, Y. Bar-Cohen, and G. M. Sessler, MRS Symposia Proceedings No. 949E (Materials Research Society, Warrendale, PA, 2007), p. 0949–C05-01.
[78]J. P. Calame, J. Appl. Phys. **99**, 084101 (2006).
[79]L. Flandin, L. Vouyovitch, A. Beroual, J. Bessede, and N. D. Alberola, J. Phys. D: Appl. Phys. **38**, 144 (2005).
[80]J. Li, Phys. Rev. Lett. **90**, 217601 (2003).
[81]J. Y. Li, L. Zhang, and S. Ducharme, Appl. Phys. Lett. **90**, 132901 (2007).
[82]Q. M. Zhang, H. F. Li, M. Poh, F. Xia, Z. Y. Cheng, H. S. Xu, and C. Huang, Nature (London) **419**, 284 (2002).